Orbital character variation of the Fermi surface and doping dependent changes of the dimensionality in $BaFe_{2-x}Co_xAs_2$ from angle-resolved photoemission spectroscopy

S. Thirupathaiah,[1] S. de Jong,[2] R. Ovsyannikov,[1] H. A. Dürr,[1,3] A. Varykhalov,[1] R. Follath,[1] Y. Huang,[2] R. Huisman,[2] M. S. Golden,[2] Yu-Zhong Zhang,[4] H. O. Jeschke,[4] R. Valentí,[4] A. Erb,[5] A. Gloskovskii,[6] and J. Fink[1,7]

[1]*Helmholtz-Zentrum Berlin, Albert-Einstein-Strasse 15, 12489 Berlin, Germany*

[2]*Van der Waals-Zeeman Institute, University of Amsterdam, NL-1018XE Amsterdam, The Netherlands*

[3]*Pulse Institute, Stanford Linear Accellerator Center, Menlo Park, California 94025, USA*

[4]*Inst. für Theor. Physik, Goethe-Universität, Max-von-Laue-Straße 1, 60438 Frankfurt, Germany*

[5]*Walther-Meissner-Institut, Walther-Meißner Strasse 8, 85748 Garching, Germany*

[6]*Institut für Anorganische Chemie und Analytische Chemie, Johannes Gutenberg-Universität, 55099 Mainz, Germany*

[7]*Leibniz-Institute for Solid State and Materials Research Dresden, P.O. Box 270116, D-01171 Dresden, Germany*

(Received 30 September 2009; revised manuscript received 15 February 2010; published 12 March 2010)

From a combination of high resolution angle-resolved photoemission spectroscopy and density functional calculations, we derive information on the dimensionality and the orbital character of the electronic states of $BaFe_{2-x}Co_xAs_2$. Upon increasing Co doping, the electronic states in the vicinity of the Fermi level take on increasingly three-dimensional character. Both the orbital variation with k_z and the more three-dimensional nature of the doped compounds have important consequences for the nesting conditions and thus possibly also for the appearance of antiferromagnetic and superconducting phases.

DOI: 10.1103/PhysRevB.81.104512 PACS number(s): 74.70.−b, 74.25.Jb, 79.60.−i, 71.20.−b

I. INTRODUCTION

Since the discovery of high T_c superconductivity in Fe pnictides,[1] many experiments have been carried out to reveal the physical and electronic properties of these materials.[2–5] The parent compounds of Fe-pnictide superconductors are antiferromagnetic (AFM) metals. Both electron and hole doping suppresses the AFM order and leads to a superconducting phase. Although it is at present not clear whether the AFM ordering can be solely mediated by nesting of hole pockets at the center of the Brillouin zone (BZ) and electron pockets at the zone corner, this nesting is certainly important for the appearance of AFM order. Nesting may be also important for the pairing mechanism in these compounds[6] although there are alternative scenarios based on the high polarizability of the As ions.[7] The nesting scenario could explain why in the SmFeAsO-based superconductors,[8] predicted to have an almost two-dimensional electronic structure,[9,10] higher superconducting transition temperatures T_c are observed than in $BaFe_2As_2$-based systems[2] which are predicted to have a more three-dimensional electronic structure.[11] In general, reduction in the dimensionality increases the number of states that could be considered to be well nested. Furthermore, we point out that the orbital character of the states at the Fermi level E_F is very important for the nesting conditions as the interband transitions which determine the electronic susceptibility, as calculated by the Lindhard function, are (in weak coupling scenarios) by far strongest when the two Fermi surfaces have the same orbital character.[12] The admixture of three-dimensionality, arising from interlayer coupling, makes the materials potentially more useful in devices and other applications. Thus the dimensionality of the electronic structure, i.e., the k_z dispersion of the electronic states is of great importance for the understanding and application of these new superconductors.

Angle-resolved photoemission spectroscopy (ARPES) is an ideal tool to study the dispersion of bands parallel and perpendicular to the FeAs layers. There exists a considerable number of experimental studies of these issues.[13–29] Nevertheless, the k_z dispersion of the near E_F states, the evolution of the electronic structure upon doping, and in particular the orbital character of the states are points of ongoing discussion and significance in relation to the microscopic mechanism for antiferromagnetism and superconductivity in these systems. In this contribution, we report a systematic study of the dimensionality of the electronic structure of $BaFe_{2-x}Co_xAs_2$ (x=0 to 0.4) using ARPES. Instrumental in uncovering two new factors which are of great significance for the nesting of the Fermi surfaces of these systems is the use of variable polarization of the synchrotron radiation. First we show that the Co doping of $BaFe_2As_2$ strongly increases the three-dimensionality of the electronic structure. Second, we also detect an important change of the orbital character of the electronic states at the Fermi level when changing the wave vector perpendicular to the layers. Our results are in qualitative agreement with density functional theory (DFT) calculations.

II. EXPERIMENTAL DETAILS

Single crystals of $BaFe_{2-x}Co_xAs_2$, were grown in Amsterdam using a self-flux method. Another set of single crystals of $BaFe_2As_2$ were grown in Garching using Sn-flux. Characterizing studies on Amsterdam samples have been reported elsewhere.[30] Crystals with actual Co concentrations x=0 (T_N=120 K), x=0.08 (T_N=55 K, T_c=13 K), x=0.17 (T_c=21 K), and x=0.4 (T_c=0 K) were studied. T_N and T_c give the Neel temperature and the superconducting transition temperature, respectively. The ARPES measurements were carried out at the BESSY II synchrotron radiation facility using the UE112-PGM2a beam line, equipped with a SCIENTA SES 100 analyzer. The total energy resolution was 25 meV while the angular resolution was 0.2° along the slit of

TABLE I. Sample alignment and Fe $3d$ orbitals which can be detected with s- and p-polarized photons.

Alignment	Fe $3d_{x^2-y^2}$	Fe $3d_{z^2}$	Fe $3d_{xz}$	Fe $3d_{yz}$	Fe $3d_{xy}$
Γ-M (p-pol)	Yes	Yes	Yes	No	No
Γ-M (s-pol)	No	No	No	Yes	Yes
Γ-X (p-pol)	No	Yes	Yes	Yes	Yes
Γ-X (s-pol)	Yes	No	Yes	Yes	No

analyzer and 0.3° perpendicular to it. All the samples were cleaved *in situ* at a temperature of less than 50 K. Further experimental details have been published previously.[31] Due to matrix element effects, measurements performed with polarized photons can detect different Fe $3d$ states depending on the polarization and sample alignment (i.e., Γ-X or Γ-M) (see Table I). In the following we will not discuss the Fe $3d_{xy}$ states as they are well below the Fermi energy E_F.

III. BAND STRUCTURE CALCULATIONS

DFT calculations have been performed on $BaFe_2As_2$ and $BaFe_{1.8}Co_{0.2}As_2$, using the Perdew-Burke-Ernzerhof generalized gradient approximation (see Fig. 1). For $BaFe_2As_2$ structural data were taken from the experiment.[32] For $BaFe_{2-x}Co_xAs_2$ we use Car-Parrinello molecular dynamics based on projector augmented wave basis to fully optimize[33] the lattice structure within the virtual crystal approximation. High symmetry points of the BZ are denoted by $\Gamma=(0,0,0)$, $Z=(0,0,1)$, $X=(1/2,1/2,0)$, $M=(1/2,0,0)$, and $K=(1/2,1/2,1)$ in the units $(2\pi/a, 2\pi/a, 2\pi/c)$, where a and c are the tetragonal lattice constants of $BaFe_2As_2$ along the x and z axis, respectively. In Fig. 1(a) and 1(b), the orbital character of the bands is shown in color.

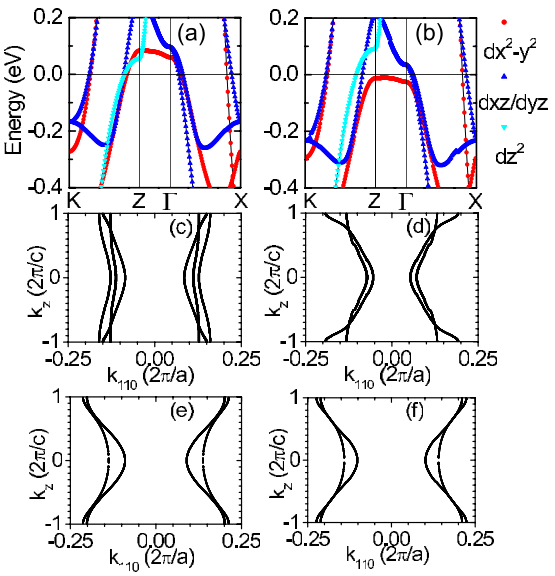

FIG. 1. (Color online) Bands and their orbital character (a) for $BaFe_2As_2$ and (b) for $BaFe_{1.8}Co_{0.2}As_2$. (c) k_z dispersion around Γ for $BaFe_2As_2$ and (d) for $BaFe_{1.8}Co_{0.2}As_2$. (e) k_z dispersion around X for $BaFe_2As_2$ and (f) for $BaFe_{1.8}Co_{0.2}As_2$.

IV. RESULTS AND DISCUSSION

ARPES measurements on undoped $BaFe_2As_2$ are displayed in Fig. 2. The measurements were performed using the photon energies $h\nu=75$ eV and $h\nu=57$ eV, corresponding to $k_z\approx 0$ (Γ point) and $k_z\approx 1$ (Z point), respectively. The k_z values are calculated using an inner potential of 15 eV.[15] s-polarized photons were used for recording the data along the Γ-X direction. Figures 2(b)–2(e) depicts the $h\nu=75$ eV data. We observe a hole pocket at Γ and an electron pocket at X in the Fermi surface map. Figure 2(c) shows the energy distribution map taken along the k_{110} direction. We resolved two bands (α_1 and α_2) at Γ. Only α_1 crosses E_F while α_2 is not visible for binding energies less than 20 meV. A Fermi vector $k_F=0.07\pm0.01$ Å^{-1} is calculated for α_1 by fitting the momentum distribution curve (MDC) taken over the integration range of a 20 meV window with respect to E_F. Using the polarization dependent selection rules (see Table I), with s-polarized photons along the Γ-X direction, the α_1 band can be attributed to x^2-y^2 and the α_2 band is related to xz and yz states. Around Γ a weak spectral feature is observed near 100 meV below E_F. This feature is related to a back folding and hybridization of bands near Γ and X, due to the orthorhombic symmetry of the lattice at low temperatures and the AFM order in the As-Fe-As block. On the other hand we could not resolve the petal- and dropletlike Fermi surfaces near Γ and X, respectively, which have been detected in the undoped antiferromagnetic systems such as $BaFe_2As_2$ (Refs. 13, 17, 22, 23, 26, and 27), $SrFe_2As_2$ (Ref. 24), and $EuFe_2As_2$ (Ref. 29). The reason for the fact that we do not resolve these reconstructions of the band structure near E_F is not clear at present. As pointed out in previous publications (see e.g., Ref. 29) along the Γ-X direction, part of the petal-like Fermi surface near Γ and the dropletlike Fermi surface near X are still reminiscent of the unreconstructed Fermi surface of the paramagnetic system. Thus the comparison—presented below—of the k_z dispersions of the undoped system and the Co doped samples, which span from AFM to paramagnetic ground states, is a valid and interesting exercise. We emphasize that the detailed study of the k_z dependent dispersion of the reconstructed Fermi surface in the antiferromagnetic state is not the main topic of this contribution and will be investigated in the future.

Around the zone corner X we observe two bands along k_{110} (α_2 and β_2) [Fig. 2(c)], and an additional electron pocket along k_{-110} (β_1) [Fig. 2(e)]. Maintaining the same geometry, but switching to $h\nu=57$ eV ($k_z\approx 1$) we can identify [Fig. 2(f)] two hole pockets around Γ and one electron pocket around X. The energy distribution map [Fig. 2(g)] shows two

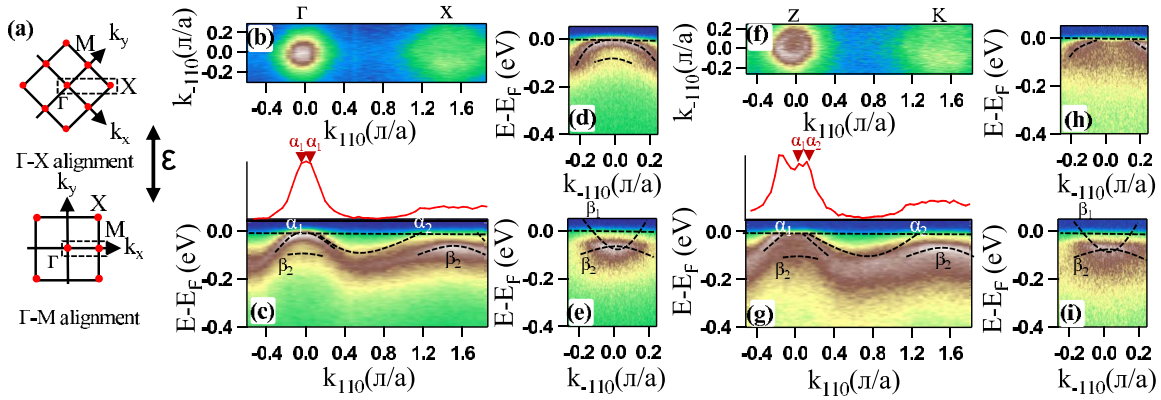

FIG. 2. (Color online) ARPES data on undoped $BaFe_2As_2$ using *s*-polarized photons measured along Γ-*X*. (a) Cartoon of sample alignment and *k* space covered. The light polarization ϵ for *s* polarization is indicated. (b)–(e) $h\nu$=75 eV, corresponding to $k_z \approx 0$ (Γ). (b) Fermi surface map, (c) energy distribution map (EDM) taken along the k_{110} direction, (d) EDM along k_{-110} around the Γ point and (e) around the *X* point. (f)–(i) Analogous data but taken with $h\nu$=57 eV, corresponding to $k_z \approx 1$ (z). The (red) curves above panel (c) and (g) represent momentum distribution curves at E_F.

bands crossing E_F at the zone center (α_1 and α_2). Since there is no clear separation between these bands we give the average Fermi vector k_F=0.11±0.01 Å^{-1}. The small difference in Fermi vectors between Γ and *Z* suggests a modest k_z dispersion in undoped $BaFe_2As_2$ a point which we will return to later.

Next we discuss our ARPES measurements on $BaFe_{1.6}Co_{0.4}As_2$, a doping level well beyond the maximal level studied in Refs. 15, 16, and 19. The data shown in Fig. 3 were recorded along Γ-*X* with $h\nu$=75 eV, corresponding to $k_z \approx 0$. Constant energy contours around Γ were taken with *p*-polarized photons [see Fig. 3(a)] and analogous contours around *X* were taken with *s*-polarized photons [Fig. 3(b)] because no spectral weight was observed at *X* with *p*-polarized photons. To resolve the band features we made different cuts along the k_{-110} direction at Γ and *X*. In Fig. 3(c) and 3(e) we can see that no bands cross E_F near Γ in these measurements performed with *p*-polarized photons. The finite spectral weight observed in Fig. 3(a) at E_F is due to the tail of the top of the valence band. Using the polarization dependent selection rules of Table I, we can thus exclude hole pockets formed from states having z^2, *xz*, or *yz* character. The existence of hole pockets with x^2-y^2 character, which according to the band structure calculations should be the first to sink below E_F upon electron doping, is excluded from measurements using *s*-polarized photons [Fig. 3(g)]. Therefore for high Co doping of $BaFe_2As_2$, the hole pockets for $k_z \approx 0$ are completely filled, i.e., there are no states at E_F near the Γ point. Furthermore, a comparison of ARPES data of $BaFe_{2-x}Co_xAs_2$ for x=0 [see Fig. 2(a)] and x=0.4 [see Fig. 3(d)] yields that the size of the electron pocket at *X* ($k_z \approx 0$) has become larger by roughly a factor of two. We mention in this context that the enlargement of the electron pockets upon Co doping is not observed for lower Co concentrations in the k_z scans depicted in Figs. 4(h)–4(j). The observed changes of the size of the electron and hole pockets for high Co concentrations could indicate a shift of E_F to higher energies upon substituting Fe by Co. On the other hand, we point out that we were not able to perform a full integration of the volume of the Fermi cylinders to judge whether a Co atom really adds one full electron to the Fe 3*d* dominated low-energy band structure.

In order to reveal the k_z dispersion of the bands in $BaFe_{2-x}Co_xAs_2$, we present in Fig. 4 photon energy dependent scans with excitation energies ranging from 42 to 108 eV in steps of 3 eV, measured near the Γ-point and the *X* point, in some cases for *s*- and *p*-polarized light and with the slit of the analyzer along different $k_\parallel$ (wave vector parallel to the surface) directions. The data are normalized to the maximum spectral weight at each photon energy which means that only relative intensities between different bands can be derived from these panels. The dots overlaid on the $h\nu$-dependent data are the result of fits to the E_F MDCs. First we focus on the undoped system. Figure 4(a) depicts the Fermi surface map in the k_{100} vs $h\nu$ plane. The data were recorded along the Γ-*M* direction with *p*-polarized light. According to Table I, in this geometry we can detect all relevant states near E_F except *yz* states. In Fig. 4(b) we show analogous data but now along the Γ-*X* direction. In this case we can detect all relevant states except the x^2-y^2 states. Finally in Fig. 4(f) we depict analogous data near Γ measured along the Γ-*X* direction with *s* polarization, under which conditions we should see all relevant states except z^2 states. Comparing Fig. 4(b) (no x^2-y^2 states) with Fig. 4(f) (no z^2 states) yields an inner modestly dispersing x^2-y^2 band, a second modestly dispersing *xz*,*yz* band with slightly larger k_F values, and near *Z* an outer z^2 band with the largest k_F value. This interpretation would be supported by the data shown in Fig. 4(a) where the photoemission matrix elements result in the signal being dominated by the x^2-y^2 and z^2 bands. This assignment agrees with the DFT band structure calculations presented here, as well as with numerous other DFT data, all of which predict a smaller k_F value at Γ for the x^2-y^2 than for the *xz*,*yz* bands. The appearance of z^2 states at the Fermi level is in accordance with our DFT calculations. Inspection of Fig. 1(a) shows that near the *Z* point there is a z^2 related Fermi surface, while near Γ, only x^2-y^2 and *xz*/*yz* states cross E_F. This k_z dependent change of the orbital character of the Fermi surface—which naturally appears in the $h\nu$-dependent ARPES intensity maps in a manner periodic in the *c*-axis

reciprocal lattice vector—combined with the strong photon energy dependence of the matrix elements for emission from z^2 states[31] gives rise to the strong intensity variations shown here and reported in Refs. 13, 15, and 23. Thus the picture for undoped $BaFe_2As_2$ is clear: there is a modest k_z dispersion of the states around $k_x=k_y=0$, but there is also an important k_z-dependent change in the orbital character of the Γ/Z-centered Fermi surfaces.

Having dealt with the important question of the dimensionality and the orbital character of the central Fermi surface cylinders of the undoped parent compound $BaFe_2As_2$, we now address the issue of the evolution of the k_z dispersion in $BaFe_{2-x}Co_xAs_2$ as a function of Co doping concentration. Figures 4(b)–4(e) show the Fermi surface maps in the k_{110} vs $h\nu$ plane, measured along Γ-X using p-polarized photons. For lower Co concentrations, by fitting the MDCs, we could resolve two bands crossing E_F around Z while at $x=0.4$ only a single band could be resolved in keeping with the data presented in Fig. 3. A remarkable observation is that with increasing Co concentration, the k_z dispersion increases and the spectral weight at Γ decreases. In the geometry used in Figs. 4(b)–4(e), we probe xz, yz, and z^2 states. Thus we relate the outer bands as in Fig. 4(b) to z^2 states while the inner ones to xz,yz states. In order to obtain more information on the orbital character of the bands, we contrast the $x=0.17$ data of Fig. 4(d), measured with p polarization, with analogous data measured with s polarization which are presented in Fig. 4(g). In the latter the spread of the spectral weight along the k_{110} direction is considerably reduced. Since in Γ-X (s-polarized) geometry, we do not detect z^2 states, and since at that doping level the x^2-y^2 band is expected to be already completely filled [see also Fig. 1(b)], we observe here only the degenerate xz,yz bands. Thus summarizing the situation for the states near the Γ point: with increasing doping concentration, first the x^2-y^2 hole pocket will be filled at x between 0.08 and 0.17, and later on the xz, yz hole pocket moves below E_F beyond $x\approx 0.2$. At Z, the x^2-y^2 pocket disappears near $x=0.2$ but there remains a hole pocket which has predominantly z^2 character. This means that with increasing doping concentration the system transforms from a more two-dimensional system with strong nesting conditions to a more three-dimensional metal where nesting is in principle possible in the $k_z=\pm 1$ planes of the BZ, but there it is strongly reduced due to the different orbital character of the Fermi surfaces. In the $k_z=0$ plane nesting is no longer possible since there is no hole pocket. The observed doping dependence of the electronic structure is in remarkable agreement with the band structure calculations [Figs. 1(c) and 1(d)].

In Figs. 4(h)–4(j) we present data measured around the X-K line with $k_\parallel$ aligned along the Γ-X (Z-K) direction with s-polarized photons for $x=0$, 0.08, and 0.17, respectively. In this specific geometry, we probe all states expected at E_F (xz, yz, and x^2-y^2). For the undoped case, the k_z dispersion is rather small which is at variance with the DFT band structure calculation shown in Fig. 1(e) but consistent with previous observations.[13,19,20] With increasing Co concentration the k_z dispersion increases. The small difference in the dispersion for the three bands is in good qualitative agreement with the calculations presented in Figs. 1(e) and 1(f).

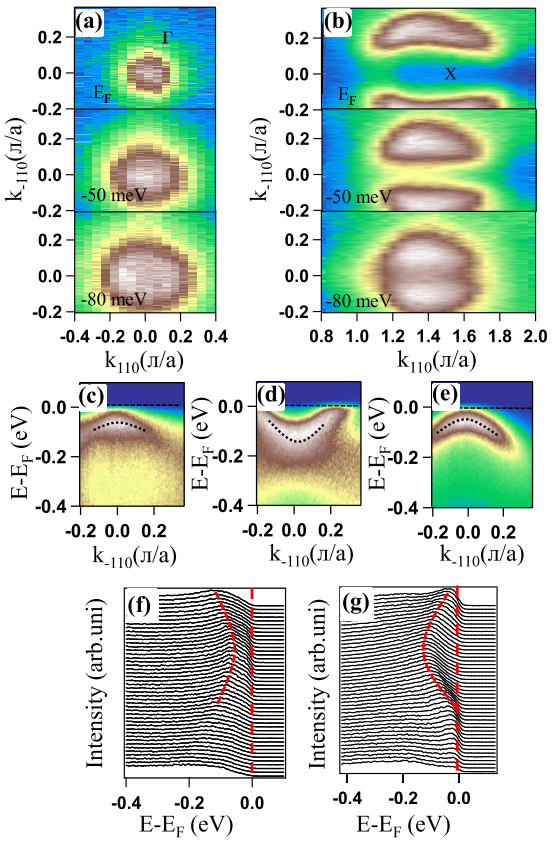

FIG. 3. (Color online) $BaFe_{1.6}Co_{0.4}As_2$ ARPES data along Γ-X. (a) and (b) constant energy maps near E_F, at E_F-50 meV, and E_F-80 meV around Γ and X, measured with p-polarized and s-polarized photons, respectively. (c) and (d) depict cuts taken along the k_{-110} direction from the center of Γ and X. (e) as in panel (c) but measured with s-polarized photons. (g) and (f) show the energy distribution curves of (c) and (d).

Before concluding the results and discussion section, we discuss relevant data in the literature, with the main focus on Co-doped $BaFe_2As_2$. In general, some of the aspects dealt with here have been reported by others, but to date this study of $BaFe_{2-x}Co_xAs_2$ is the only one combining three important factors: (i) a broad range in Co doping levels (going beyond the $x=0.2$ or $x=0.3$ reported so far in Refs. 15 and 16, respectively), (ii) a broad range in photon energies used, thereby enabling a full picture of the k_z dependencies to be determined (iii) exploitation of variable polarization of synchrotron radiation, so as to enable an orbital analysis of the Fermi surfaces.

As regards publications dealing with the k_z dependence of the electronic states of MFe_2As_2 compounds, Ref. 13 deals with $h\nu$ dependence for $CaFe_2As_2$, but the lack of polarization dependent data means that if the orbital polarization change shown in our work to be taking place between $k_z=0$ and $k_z=1$ would also occur for $CaFe_2As_2$, then the fact that it would then go unremarked in Ref. 13 could result in an overestimation of the k_z dispersion of the Γ-centered FS's, and may underlie the claim made for a three-dimensional (3D) to two-dimensional (2D) transition on going from the orthorhombic (low temperature, antiferromagnetic) to tetragonal (high temperature, paramagnetic) phases. A similar situ-

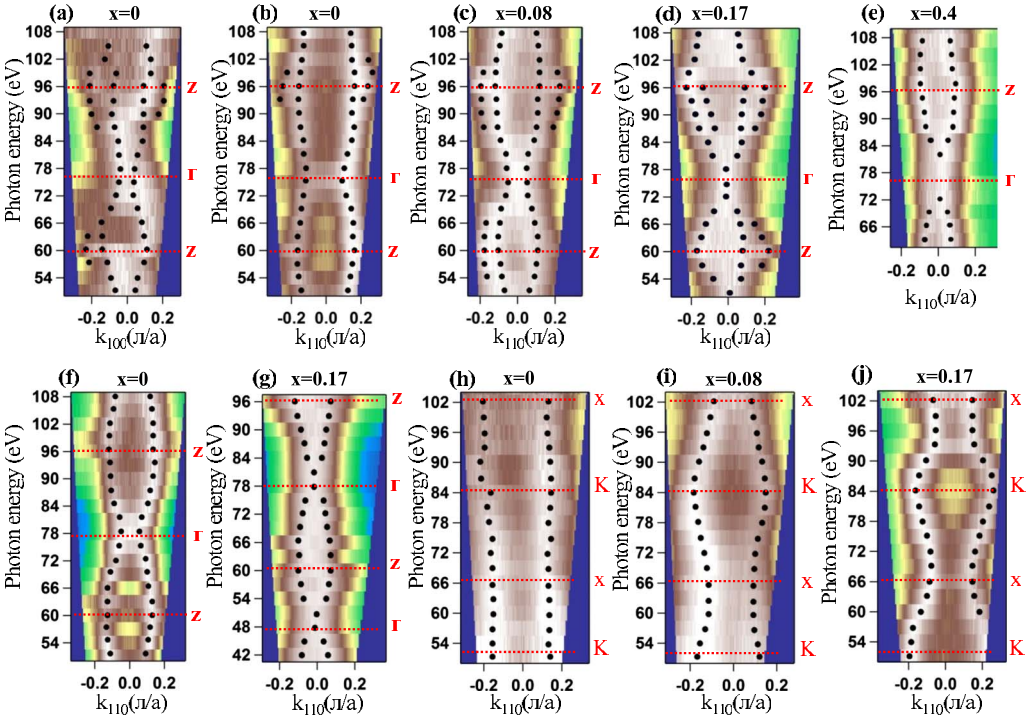

FIG. 4. (Color online) Photon energy dependent ARPES measurements performed on $BaFe_{2-x}Co_xAs_2$ to reveal the k_z dispersion as a function of doping concentration. (a) Fermi surface for $x=0$, in the k_{100} vs $h\nu$ plane near $k_x=k_y=0$ measured with p-polarized photons. (b) Analogous data as in (a) but in the k_{110} vs $h\nu$ plane. (c), (d), and (e): analogous data as in (b) but for $x=0.8$, 0.17, and 0.4, respectively. (f) and (g): analogous data as (b) but measured with s-polarized photons for $x=0$ and 0.17. (h), (i), and (j) Fermi surfaces in the k_{110} vs $h\nu$ plane near $k_x=k_y=1$ measured with s-polarized photons for $x=0$, 0.08, and 0.17, respectively.

ation as regards the effect of the orbital polarization changes with k_z is to be expected in the $h\nu$-dependent Co-doped $BaFe_2As_2$ data of Ref. 15.

Reference 16 deals with Co-doped $BaFe_2As_2$, concentrating on using helium lamp data (i.e., recorded with radiation with a fixed, low degree of polarization) to compare the Co doping levels $x=0.15$ and 0.3. The single photon energy used and the lack of polarization dependence allow no experimental statements to be made about the three-dimensionality and orbital character of the states in question. For the k_z value accessed, a single Γ-centered holelike FS is observed for $x=0.15$ and no holelike FS's at Γ for $x=0.3$.

Reference 17 compares K doped $BaFe_2As_2$ with the undoped compound and $x=0.12$ Co doping, without use of a broad photon energy range to examine k_z dependencies, nor polarization dependence for an orbital analysis. For the Co-doped case the hole pockets at Γ are seen to shrink upon Co doping.

Reference 19 compares Co-doped $BaFe_2As_2$ with $x=0$ and 0.14, both measured across a wide photon energy range for a single polarization. Shrinkage of the holelike pockets at the zone center is reported upon Co doping, and the band dispersions and Fermi surfaces around Γ are found to be strongly photon energy dependent, and though the authors mention from the point of view of their band structure calculations that the z^2-related Fermi surfaces are the most modulated in k_z, they are not able to present an orbital analysis via the polarization dependence of the experimental data.

Reference 20 presents a thorough study of Co-doped $BaFe_2As_2$ covering a wide range of photon energies for doping levels up to $x=0.6$. Fermi wave vectors are derived from linear extrapolations of the dispersion relations. The authors mention that taken at face value, their Co doped data suggest a strong modulation of the larger holelike Fermi surface with k_z, which agrees with our data. However, it is also mentioned in Ref. 20 that it cannot be ruled out that the relevant Fermi surface loses weight for k_z values at the zone center and equivalent points. Indeed, the polarization dependent analysis presented here, coupled to the insight as regards the orbital polarization changes at $k_z=0$ and 1 from our DFT calculations offer a consistent explanation: for $k_z=1$, the outermost holelike FS is of z^2 character, whereas for $k_z=0$ it is of xz/yz character. In our earlier study,[31] we already learned that the z^2 bands carry very little weight for k_z values near zero. This means (a) that some of the estimates of k_F vectors and hole concentrations presented in Ref. 20 could probably be revised and (b) the "counterintuitive" fact that the hole pocket with k_F matching that of the electron pocket for the antiferromagnetic, low Co-doped systems seemed to be one displaying significant 3D character, is no longer a problem, as our data show that for low doping, the 3D character is, in fact, modest.

V. CONCLUSION

We have performed a systematic photon energy dependent, high resolution ARPES study to reveal the intrinsic k_z dispersion in $BaFe_{2-x}Co_xAs_2$, covering a doping range of up to $x=0.4$. By combining the insight gained from an orbital

analysis of the FS's with our DFT data and previous knowledge of the k_z dependence of the matrix elements for certain states,[31] we are able to state that in these data from the undoped system we see a modest k_z dispersion near $k_x=k_y=0$. At higher Co doping the k_z dispersion increases and a gradual filling of all three hole pockets at Γ is detected. This means that as Co doping proceeds, the nesting conditions are strongly reduced within the $k_z=0$ plane and thereabouts. This is all the more significant, in the light of the fact that nesting in the $k_z=1$ plane at higher Co concentrations would require interband transitions between states of differing orbital symmetry (z^2 at Z and $xz/yz/x^2-y^2$ at K). Thus, the combination of the Fermi surface shrinkage at Γ as a result of electron doping with the k_z-dependent orbital polarization results in a situation in which the warped Fermi surface cylinders for optimally doped superconducting $BaFe_{2-x}Co_xAs_2$ are most likely best nested across wave vectors containing a significant k_z component. This could lie at the root of the robust three-dimensionality of the superconducting properties of these systems. Furthermore, our combination of ARPES and DFT data could provide a microscopic explanation for the disappearance of superconductivity for x at or greater than 0.36,[34] as by this doping the Γ-centered holelike Fermi surfaces are all fully below E_F and interband scattering with wave vectors $(\pi/a,\pi/a,0)$ involving like Fe $3d$ orbitals are closed off. The results on the dimensionality have also implication for the potential application of these materials.

ACKNOWLEDGMENTS

We acknowledge the characterization of single crystals by H. Luigjes. Financial support by the DFG is appreciated by J.F. (Forschergruppe FOR 538). This work is part of the research program of the "Stichting voor Fundamenteel Onderzoek der Materie (FOM)," which is financially supported by the "Nederlandse Organisatie voor Wetenschappelijk Onderzoek (NWO)."

[1] Y. Kamihara, T. Watanabe, M. Hirano, and H. Hosono, J. Am. Chem. Soc. **130**, 3296 (2008).
[2] M. Rotter, M. Tegel, and D. Johrendt, Phys. Rev. Lett. **101**, 107006 (2008).
[3] X. F. Wang, T. Wu, G. Wu, H. Chen, Y. L. Xie, J. J. Ying, Y. J. Yan, R. H. Liu, and X. H. Chen, Phys. Rev. Lett. **102**, 117005 (2009).
[4] H. Q. Yuan, J. Singleton, F. F. Balakirev, S. A. Baily, G. F. Chen, J. L. Luo, and N. L. Wang, Nature (London) **457**, 565 (2009).
[5] M. A. Tanatar, N. Ni, C. Martin, R. T. Gordon, H. Kim, V. G. Kogan, G. D. Samolyuk, S. L. Bud'ko, P. C. Canfield, and R. Prozorov, Phys. Rev. B **79**, 094507 (2009).
[6] I. I. Mazin, D. J. Singh, M. D. Johannes, and M. H. Du, Phys. Rev. Lett. **101**, 057003 (2008).
[7] G. A. Sawatzky, I. S. Elfimov, J. van den Brink, and J. Zaanen, EPL **86**, 17006 (2009).
[8] R. H. Liu, G. Wu, T. Wu, D. F. Fang, H. Chen, S. Y. Li, K. Liu, Y. L. Xie, X. F. Wang, R. L. Yang *et al.*, Phys. Rev. Lett. **101**, 087001 (2008).
[9] D. J. Singh and M.-H. Du, Phys. Rev. Lett. **100**, 237003 (2008).
[10] F. Ma and Z.-Y. Lu, Phys. Rev. B **78**, 033111 (2008).
[11] D. J. Singh, Phys. Rev. B **78**, 094511 (2008).
[12] S. Graser, T. A. Maier, P. J. Hirschfeld, and D. J. Scalapino, New J. Phys. **11**, 025016 (2009).
[13] C. Liu, T. Kondo, N. Ni, A. D. Palczewski, A. Bostwick, G. D. Samolyuk, R. Khasanov, M. Shi, E. Rotenberg, S. L. Bud'ko, P. C. Canfield, and A. Kaminski, Phys. Rev. Lett. **102**, 167004 (2009).
[14] V. Zabolotnyy, D. Inosov, B. Evtushinski, A. Koitzsch, A. Kordyuk, J. Park, D. Haug, V. Hinkov, A. Boris, G. Sun, J. T. Park, D. Haug, V. Hinkov, A. V. Boris, C. T. Lin, M. Knupfer, A. N. Yaresko, B. Büchner, A. Varykhalov, R. Follath, and S. V. Borisenko, Nature (London) **457**, 569 (2009).
[15] P. Vilmercati, A. Fedorov, I. Vobornik, U. Manju, G. Panaccione, A. Goldoni, A. S. Sefat, M. A. McGuire, B. C. Sales, R. Jin, D. Mandrus, D. J. Singh, and N. Mannella, Phys. Rev. B **79**, 220503(R) (2009).
[16] Y. Sekiba, T. Sato, K. Nakayama, K. Terashima, P. Richard, J. H. Bowen, H. Ding, Y.-M. Xu, L. J. Li, G. H. Cao, Z.-A. Xu, and T. Takahashi, New J. Phys. **11**, 025020 (2009).
[17] M. Yi, D. H. Lu, J. G. Analytis, J. H. Chu, S. K. Mo, R. H. He, X. J. Zhou, G. F. Chen, J. L. Luo, N. L. Wang, Z. Hussain, D. J. Singh, I. R. Fisher, and Z.-X. Shen, Phys. Rev. B **80**, 024515 (2009).
[18] M. Yi, D. H. Lu, J. G. Analytis, J.-H. Chu, S.-K. Mo, R.-H. He, M. Hashimoto, R. G. Moore, I. I. Mazin, D. J. Singh, Z. Hussain, I. R. Fisher, and Z.-X. Shen, Phys. Rev. B **80**, 174510 (2009).
[19] W. Malaeb, T. Yoshida, A. Fujimori, M. Kubota, K. Ono, K. Kihou, P. M. Shirage, H. Kito, A. Iyo, H. Eisaki, Y. Nakajima, T. Tamegai, and R. Arita, J. Phys. Soc. Jpn. **78**, 123706 (2009).
[20] V. Brouet, M. Marsi, B. Mansart, A. Nicolaou, A. Taleb-Ibrahimi, P. Le Fevre, F. Bertran, F. Rullier-Albenque, A. Forget, and D. Colson, Phys. Rev. B **80**, 165115 (2009).
[21] L. X. Yang, Y. Zhang, H. W. Ou, J. F. Zhao, D. W. Shen, B. Zhou, J. Wei, F. Chen, M. Xu, C. He, Y. Chen, Z. D. Wang, X. F. Wang, T. Wu, G. Wu, X. H. Chen, M. Arita, K. Shimada, M. Taniguchi, Z. Y. Lu, T. Xiang, and D. L. Feng, Phys. Rev. Lett. **102**, 107002 (2009).
[22] Y. Zhang, J. Wei, H. W. Ou, J. F. Zhao, B. Zhou, F. Chen, M. Xu, C. He, G. Wu, H. Chen, M. Arita, K. Shimada, H. Namatame, M. Taniguchi, X. H. Chen, and D. L. Feng, Phys. Rev. Lett. **102**, 127003 (2009).
[23] T. Kondo, R. M. Fernandes, R. Khasanov, C. Liu, A. D. Palczewski, N. Ni, M. Shi, A. Bostwick, E. Rotenberg, J. Schmalian, S. L. Bud'ko, P. C. Canfield, and A. Kaminski, Phys. Rev. B **81**, 060507(R) (2010).
[24] D. Hsieh, Y. Xia, L. Wray, D. Qian, K. Gomes, A. Yazdani, G. Chen, J. Luo, N. Wang, and M. Hasan, arXiv:0812.2289 (unpublished).
[25] Y. Zhang, B. Zhou, F. Chen, J. Wei, M. Xu, L. Yang, C. Fang, W. Tsai, G. Cao, Z. Xu, M. Arita, C. Hong, K. Shimada, H. Nama-

tame, M. Taniguchi, J. Hu, and D. Feng, arXiv:0904.4022 (unpublished).

[26] T. Shimojima, K. Ishizaka, Y. Ishida, N. Katayama, K. Ohgushi, T. Kiss, M. Okawa, T. Togashi, X. Wang, C.-T. Chen, S. Watanabe, R. Kadota, T. Oguchi, A. Chainani, and S. Shin, Phys. Rev. Lett. **104**, 057002 (2010).

[27] P. Richard, K. Nakayama, T. Sato, M. Neupane, Y. M. Xu, J. H. Bowen, G. F. Chen, J. L. Luo, N. L. Wang, H. Ding, *et al.*, arXiv:0909.0574 (unpublished).

[28] C. Liu, T. Kondo, R. Fernandes, A. Palczewski, E. Mun, N. Ni, A. Thaler, A. Bostwick, E. Rotenberg, J. Schmalian, S. Budko, P. Canfield, and A. Kaminski, arXiv:0910.1799 (unpublished).

[29] S. de Jong, E. van Heumen, S. Thirupathaiah, R. Huisman, F. Massee, J. B. Goedkoop, R. Ovsyannikov, J. Fink, H. A. Duerr, A. Gloskovskii *et al.*, EPL **89**, 27007 (2010).

[30] F. Massee, Y. Huang, R. Huisman, S. de Jong, J. B. Goedkoop, and M. S. Golden, Phys. Rev. B **79**, 220517(R) (2009).

[31] J. Fink, S. Thirupathaiah, R. Ovsyannikov, H. A. Duerr, R. Follath, Y. Huang, S. de Jong, M. S. Golden, Y.-Z. Zhang, H. O. Jeschke, R. Valentí, C. Felser, S. Dastjani Farahani, M. Rotter, and D. Johrendt, Phys. Rev. B **79**, 155118 (2009).

[32] Q. Huang, Y. Qiu, W. Bao, M. A. Green, J. W. Lynn, Y. C. Gasparovic, T. Wu, G. Wu, and X. H. Chen, Phys. Rev. Lett. **101**, 257003 (2008).

[33] Y.-Z. Zhang, H. C. Kandpal, I. Opahle, H. O. Jeschke, and R. Valentí, Phys. Rev. B **80**, 094530 (2009).

[34] J.-H. Chu, J. G. Analytis, C. Kucharczyk, and I. R. Fisher, Phys. Rev. B **79**, 014506 (2009).